We are IntechOpen, the world's leading publisher of Open Access books Built by scientists, for scientists

5,300
Open access books available

130,000
International authors and editors

155M
Downloads

154
Countries delivered to

Our authors are among the

TOP 1%
most cited scientists

12.2%
Contributors from top 500 universities

CLARIVATE ANALYTICS

BOOK CITATION INDEX

INDEXED

WEB OF SCIENCE™

Selection of our books indexed in the Book Citation Index
in Web of Science™ Core Collection (BKCI)

Interested in publishing with us?
Contact book.department@intechopen.com

Numbers displayed above are based on latest data collected.
For more information visit www.intechopen.com

Modeling of the Flexible Needle Insertion into the Human Liver

Veturia Chiroiu, Ligia Munteanu, Cristian Rugină and Nicoleta Nedelcu

Abstract

The insertion of the needle is difficult because the deformation and displacement of the organs are the key elements in the surgical act. Liver and tumor modeling are essential in the development of the needle insertion model. The role of the needle is to deliver into the tumor an active chemotherapeutic agent. We describe in this chapter the deformation of the needle during its insertion into the human liver in the context of surgery simulation of the high- robotic-assisted intraoperative treatment of liver tumors based on the integrated imaging-molecular diagnosis. The needle is a bee barbed type modeled as a flexible thread within the framework of the Cosserat (micropolar) elasticity theory.

Keywords: bee needle, human liver, Cosserat elasticity theory

1. Introduction

The flexible bee needles are useful tools to transport drugs into the liver tumors [1, 2]. The insertion trajectory of the needle must avoid the ribs, blood vessels, and other organs to protect the liver [3–6] (**Figure 1a**). The bee needle assures reduced insertion forces and small tissue deformations because of the tip deflections. The furthermost current publications on the surgical needle navigation into the liver can be demonstrated in [7–9]. The bee needle is shown in **Figure 1b**. The front angle has 157 deg., the back angle, 110 deg., the height is 0.5 mm, and the tip thickness 0.15 mm.

A number of scientific researches have been carried out on the collision free trajectory of the needle to the target. The surgical event requires experience in imaging the tumor location based on the liver structure and the microstructural interaction between the needle and the liver. Several studies have revealed that the needle flexibility is essential to achieve a good precision in the handling.

The strain and stress fields and the topological changes of the liver are not to be neglected during the needle navigation towards the tumor [10–13]. Details of the forces during needle insertion into the liver are find in [14], the real time collision detection for virtual surgery in [15] and the minimal hierarchical collision detection in [16]. Optimization is required to modify the needle trajectory in order to protect the liver [17, 18], to manage the tumor risk [19], and to change the robot architecture [20–22]. The inverse sonification problem for capturing hardly detectable details in a medical image is treated in [23], and the control in [24–27]. Microscopic investigation of the human liver offers details on its microanatomy with emphases
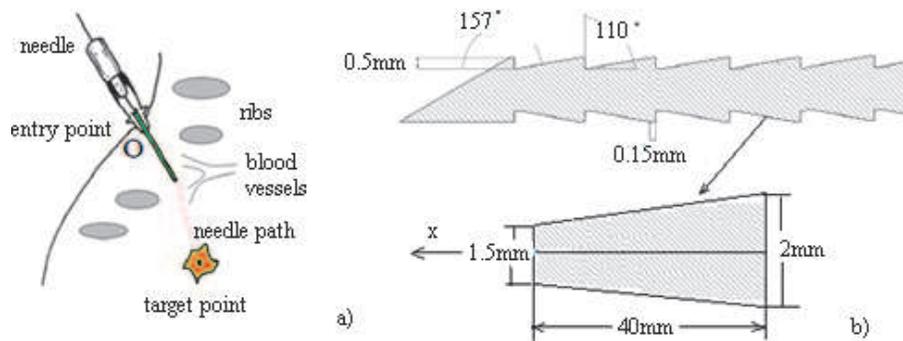
Figure 1.
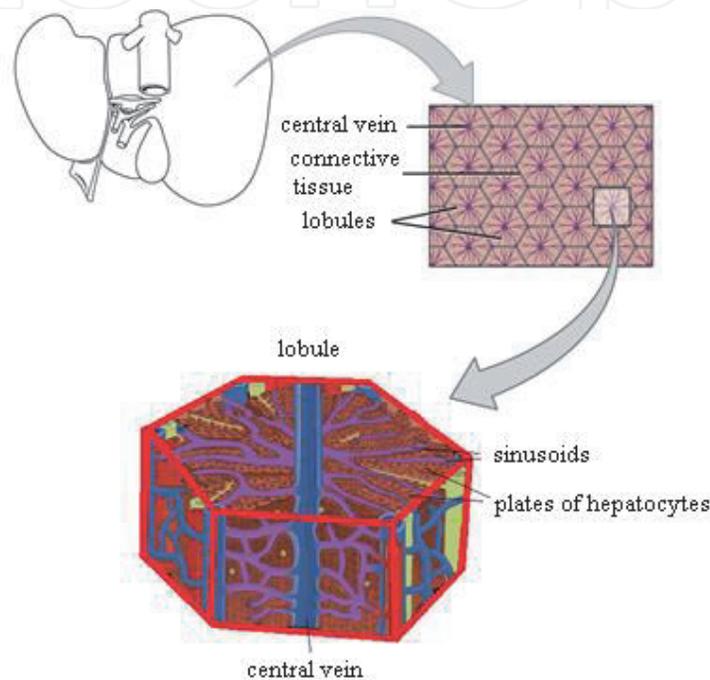*a) Trajectory towards the liver tumor; b) honeybee barbed needle [1, 2].*

Figure 2.
Hepatic lobule - basic unit of the liver.

to the granular, fibrillar components and irregular solid–fluid interfaces [28–30]. The basic unit of the liver is the hepatic lobule which is a hexagonal element with comprised the portal triad -portal vein, hepatic artery and the bile duct [31, 32]. Lobuli form two layers membranes with internal space of 100A and the cellular elements with twisted, spiraling fibers braided into the helical and screw-shaped gaps (pores) of 40–100 μm in size (**Figure 2**) [33–36].

In this chapter we try to answer a few questions such as how is the deformation of the needle and how the free-collision trajectories are determined.

2. Deformation of the needle

The needle is a bee barbed needle and it is modeled as a flexible thread within the framework of the Cosserat (micropolar) elasticity theory [37–42]. The Cosserat elasticity is applied to describe the interaction between the needle and the human liver. Let us consider a serial surgical robot composed of a revolute joint and a flexible needle. A Lagrange frame (X, Y, Z) of base vectors (e_1, e_2, e_3) and origin O in the entry point of the skin is attached to the robot (**Figure 3**). The Euler frame $K(x, y, z)$ with origin in the joint and the base vectors (d_1, d_2, d_3) is attached to the
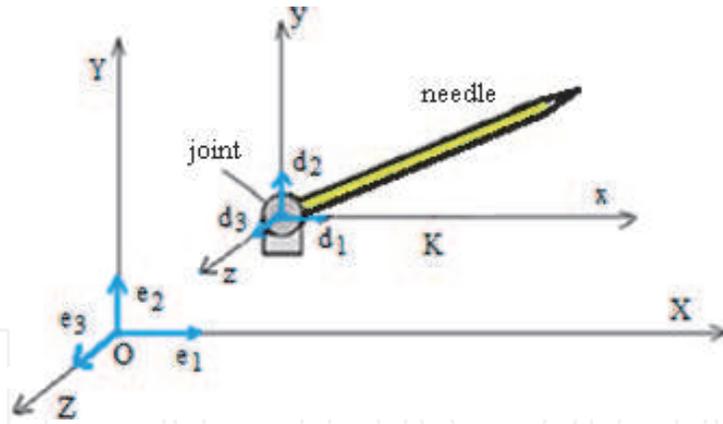
Figure 3.
Lagrange coordinate system OXYZ and the Euler coordinate system oxyz attached to the needle.

needle. The angle between the flexible arm and axis x is θ. Bending and torsion of the needle are described by the strain functions (u_1, u_2, u_3). The robot has f degrees of freedom $f = f_r + f_e$, where $f_r = 1$ is the generalized coordinate of the rigid system and $f_e = 3$ are the degrees of freedom of the flexible needle [43, 44].

The Euler axes are oriented with respect to the Lagrange axes by Euler angles υ, ψ and φ [43].

$$
\begin{aligned}
d_1 &= (-\sin\psi\sin\varphi + \cos\psi\cos\varphi\cos\upsilon)e_1 + \\
&\quad + (\cos\psi\sin\varphi + \sin\psi\cos\varphi\cos\upsilon)e_2 - \sin\upsilon\cos\varphi e_3, \\
d_2 &= (-\sin\psi\cos\varphi - \cos\psi\sin\varphi\cos\upsilon)e_1 + \\
&\quad + (\cos\psi\cos\varphi - \sin\psi\sin\varphi\cos\upsilon)e_2 + \sin\upsilon\sin\varphi e_3, \\
d_3 &= \sin\upsilon\cos\psi e_1 + \sin\upsilon\sin\psi e_2 + \cos\upsilon\, e_3.
\end{aligned}
\tag{1}
$$

The functions (u_1, u_2, u_3) measure the bending and torsion of the needle as

$$
\begin{aligned}
u_1 &= \upsilon'\sin\varphi - \psi'\sin\upsilon\cos\varphi, \\
u_2 &= \upsilon'\cos\varphi + \psi'\sin\upsilon\sin\varphi, \\
u_3 &= \varphi' + \psi'\cos\upsilon,
\end{aligned}
\tag{2}
$$

where $(')$ means the partial differentiation with respect to s which is the coordinate along the central line of the needle. The functions u_1 and u_2 describe the bending of the needle, and the function u_3 the torsion of the needle. In addition, u_1 and u_2 are components of the curvature κ of the central line corresponding to the planes (yz) and (xz)

$$
\kappa^2 = u_1^2 + u_2^2 = \upsilon'^2 + \psi'^2\sin^2\upsilon.
\tag{3}
$$

The function u_3 measures the torsion τ of the needle

$$
u_3 = \tau = \varphi' + \psi'\cos\upsilon.
\tag{4}
$$

So, the needle is rigid along the tangential direction and the total length of the needle l is invariant, the ends being fixed by the force $F = -f$ with $f = (f_1, f_2, f_3)$. This force describes the contact between the needle and the tissue $f = p_c n = p_c g'$, where g is a gap function with respect to s.

The link between the position vector $r = (x, y, z)$ and unit tangential vector d_3 is $r = \int_0^s d_3 \, ds$, or

$$x(s) = \int_0^s \cos\psi \sin\upsilon \, ds, \; y(s) = \int_0^s \sin\psi \sin\upsilon \, ds, \; z(s) = \int_0^s \cos\upsilon \, ds. \tag{5}$$

We introduce the inertia of the needle characterized by

$$(\rho_0 A_0)(s), (\rho_0 I_1)(s), (\rho_0 I_2(s)), \tag{6}$$

where ρ_0 is the mass density per unit volume, A_0 the area of the cross section, I_1, I_2 are geometrical moments of inertia around the axis, which is perpendicular to the central axis and respectively around the central axis.

The equations which describe the deformation are

$$-\rho \ddot{r} - \lambda' = 0, \tag{7}$$

$$\begin{aligned}
&k_1 \left(\dot{\psi}^2 \sin\upsilon \cos\upsilon - \ddot{\upsilon} \right) - k_2 (\dot{\varphi} + \dot{\psi} \cos\upsilon) \dot{\psi} \sin\upsilon - \\
&- A \left(\psi'^2 \sin\upsilon \cos\upsilon - \upsilon'' \right) + C(\varphi' + \psi' \cos\upsilon)\psi' \sin\upsilon - \\
&- \lambda_1 \cos\upsilon \cos\psi - \lambda_2 \cos\upsilon \sin\psi + \lambda_3 \sin\upsilon = 0,
\end{aligned} \tag{8}$$

$$\begin{aligned}
&- \frac{\partial}{\partial t} \left\{ k_1 \dot{\psi} \sin^2\upsilon + k_2 (\dot{\varphi} + \dot{\psi} \cos\upsilon) \cos\upsilon \right\} + \\
&+ \frac{\partial}{\partial s} \left\{ A\psi'^2 \sin^2\upsilon + C(\varphi' + \psi' \cos\upsilon) \cos\upsilon \right\} + \\
&+ \lambda_1 \sin\upsilon \sin\psi - \lambda_2 \sin\upsilon \cos\psi = 0,
\end{aligned} \tag{9}$$

$$-k_2 \frac{\partial}{\partial t} (\dot{\varphi} + \dot{\psi} \cos\upsilon) + C\frac{\partial}{\partial s}(\varphi' + \psi' \cos\upsilon) = 0. \tag{10}$$

where A and C are the bending stiffness and respectively the torsional stiffness of the needle, related to the Lame constants λ, μ by $A = \frac{1}{4}\pi a^4 E, C = \frac{1}{2}\pi a^4 \mu, A = \frac{1}{4}\pi a^4 E, C = \frac{1}{2}\pi a^4 \mu$, where $E = \frac{\mu(3\lambda+2\mu)}{\lambda+\mu}$ is the Young's elastic modulus, and a is the radius of the cross section of the needle, and

$$\rho = A_0\rho_0 = \pi a^2 \rho_0, k_1 = I_1 \rho_0 = \frac{\pi a^4}{4}\rho_0, k_2 = I_2\rho_0 = \frac{\pi a^4}{2}\rho_0. \tag{11}$$

The Eqs. (7–11) are solved by using the cnoidal method [43].

In short, this method is reducible to a generalization of the Fourier series with the cnoidal functions as the fundamental basis function. This is because the cnoidal functions are much richer than the trigonometric or hyperbolic functions, that is, the modulus m of the cnoidal function, $0 \leq m \leq 1$, can be varied to obtain a sine or cosine function ($m \cong 0$), a Stokes function ($m \cong 0.5$) or a solitonic function, sech or tanh.

To understand the cnoidal method, consider now a nonlinear system of equations that govern the motion of a dynamical system

$$\frac{d\theta_i}{dt} = F_i(\theta_1, \theta_2, \ldots, \theta_n), i = 1, \ldots, n, n \geq 3, \tag{12}$$

with $x \in \mathbb{R}^n$, $t \in [0, T]$, $T \in \mathbb{R}$, where F may be of the form

$$
\begin{aligned}
F_i = & \sum_{p=1}^{n} a_{ip}\theta_p + \sum_{p,q=1}^{n} b_{ipq}\theta_p\theta_q + \sum_{p,q,r=1}^{n} c_{ipqr}\theta_p\theta_q\theta_r + \\
& + \sum_{p,q,r,l=1}^{n} d_{ipqrl}\theta_p\theta_q\theta_r\theta_l + \sum_{p,q,r,l,m=1}^{n} e_{ipqrlm}\theta_p\theta_q\theta_r\theta_l\theta_m + \ldots,
\end{aligned}
\tag{13}
$$

where $i = 1, 2, \ldots, n$, and $a, b, c \ldots$ constants.

This system of equations can be reduced to Weierstrass equations of the type

$$
\dot{\theta}_2 = P_n(\theta),
\tag{14}
$$

We introduce the function transformation

$$
\theta = 2 \frac{d^2}{dt^2} \log \Theta_n(t),
\tag{15}
$$

where the theta function $\Theta_n(t)$ are defined as

$$
\begin{aligned}
\Theta_1 = & 1 + \exp(i\omega_1 t + B_{11}), \\
\Theta_2 = & 1 + \exp(i\omega_1 t + B_{11}) + \exp(i\omega_2 t + B_{22}) + \exp(\omega_1 + \omega_2 + B_{12}), \\
\Theta_3 = & 1 + \exp(i\omega_1 t + B_{11}) + \exp(i\omega_2 t + B_{22}) + \\
& + \exp(i\omega_3 t + B_{33}) + \exp(\omega_1 + \omega_2 + B_{12}) + \\
& + \exp(\omega_1 + \omega_3 + B_{13}) + \exp(\omega_2 + \omega_3 + B_{23}) + \\
& + \exp(\omega_1 + \omega_2 + \omega_3 + B_{12} + B_{13} + B_{23}),
\end{aligned}
\tag{16}
$$

and

$$
\Theta_n = \sum_{M \in (-\infty, \infty)} \exp\left(i \sum_{i=1}^{n} M_i \omega_i t + \frac{1}{2} \sum_{i<j}^{n} B_{ij} M_i M_j \right),
\tag{17}
$$

$$
\exp B_{ij} = \left(\frac{\omega_i - \omega_j}{\omega_i + \omega_j} \right)^2, \quad \exp B_{ii} = \omega_i^2.
\tag{18}
$$

Further, we write the solution (15) under the form

$$
\theta(t) = 2 \frac{\partial^2}{\partial t^2} \log \Theta_n(\eta) = \theta_{lin}(\eta) + \theta_{int}(\eta),
\tag{19}
$$

for $\eta = -\omega t + \phi$. The first term θ_{lin} represents a linear superposition of cnoidal waves. Indeed, after a little manipulation and algebraic calculus, obtain

$$
\theta_{lin} = \sum_{l=1}^{n} \alpha_l \left[\frac{2\pi}{K_l \sqrt{m_l}} \sum_{k=0}^{\infty} \left[\frac{q_l^{k+1/2}}{1 + q_l^{2k+1}} \cos(2k+1) \frac{\pi \omega_l t}{2 K_l} \right]^2 \right].
\tag{20}
$$

In (20) we recognize the expression [43].

$$
\theta_{lin} = \sum_{l=1}^{n} \alpha_l \operatorname{cn}^2[\omega_l t; m_l],
\tag{21}
$$

with

$$q = \exp\left(-\pi \frac{K'}{K}\right),$$

$$K = K(m) + \int_0^{\pi/2} \frac{du}{\sqrt{1 - m \sin^2 u}},$$

$$K'(m_1) = K(m), m + m_1 = 1.$$

The second term θ_{int} represents a nonlinear superposition or interaction among cnoidal waves. We write this term as

$$2 \frac{d^2}{dt} \log\left[1 + \frac{F(t)}{G(t)}\right] \approx \frac{\beta_k \, cn^2(\omega t, m_k)}{1 + \gamma_k \, cn^2(\omega t, m_k)}. \tag{22}$$

If m_k take the values 0 or 1, the relation (22) is directly verified. For $0 \le m_k \le 1$, the relation is numerically verified with an error of $|e| \le 5 \times 10^{-7}$. Consequently, we have

$$\theta_{nonlin} = \frac{\sum_{k=0}^n \beta_k \, cn^2[\eta; m_k]}{1 + \sum_{k=0}^n \lambda_k \, cn^2[\eta; m_k]}. \tag{23}$$

As a result, the cnoidal method yields to solutions consisting of a linear superposition and a nonlinear superposition of cnoidal waves.

Therefore, by applying the cnoidal method, the closed form solutions of the Euler angles θ, ψ and φ are obtained [43].

$$\cos \upsilon = \zeta = \zeta_2 - (\zeta_2 - \zeta_3)cn^2\left(\sqrt{\frac{|\lambda_3|}{2A}(\zeta_1 - \zeta_3)}(\xi - \xi_3), m\right) = \tag{24}$$

$$= \zeta_2 - (\zeta_2 - \zeta_3)cn^2[w(\xi - \xi_3), m],$$

where $m = \frac{\zeta_2 - \zeta_3}{\zeta_1 - \zeta_3}$ and $w = \sqrt{\frac{|\lambda_3|}{2A}(\zeta_1 - \zeta_3)}$,

$$\psi = \frac{1}{4(A - k_1 v^2)^2 w^2}\left\{-\frac{\beta + (C - k_2 v^2)\tau}{1 - \zeta_3}\prod\left[w(\xi - \xi_3), \frac{\zeta_2 - \zeta_3}{1 - u_3}, m\right] - \right.$$
$$\left. -\frac{\beta - (C - k_2 v^2)\tau}{1 + \zeta u_3}\prod\left[w(\xi - \xi_3), \frac{\zeta_2 - \zeta_3}{1 + u_3}, m\right]\right\}, \tag{25}$$

$$\varphi = -\frac{\tau[C - A - (k_2 + k_1)v^2]}{A - k_1 v^2}\xi + \frac{1}{4(A - k_1 v^2)^2 w^2}\left\{\frac{\beta + (C - k_2 v^2)\tau}{1 - \zeta_3} \times \right.$$

$$\left. \times \prod\left[w(\xi - \xi_3), \frac{\zeta_2 - \zeta_3}{1 - \zeta_3}, m\right] - \frac{\beta - (C - k_2 v^2)\tau}{1 + \zeta_3}\prod\left(w(\xi - \xi_3), \frac{\zeta_2 - \zeta_3}{1 + \zeta_3}, m\right)\right\}, \tag{26}$$

with $\prod(x, z, m) = \int_0^x \frac{dy}{1 - z \, sn^2(y, m)}$ the normal elliptic integral of the third kind.

Functions $\zeta_1, \zeta_2, \zeta_3$ are solutions of the equation

$$\frac{1}{2}\zeta'^2 = a\zeta^3 + b\zeta^2 - a\zeta + c, \tag{27}$$

$$a = -\frac{\lambda_3}{A} \neq 0, b = \frac{1}{2A}\left(\gamma - \frac{C^2\tau^2}{A}\right), c = -\frac{1}{2A}\left(\gamma - \frac{\beta^2}{A}\right). \tag{28}$$

Our objective is to determine the functions which measure the bending of the needle (u_1 and u_2), and the torsion (u_3). To visualize the strain profile of the needle, we chose two routes (**Figure 4**). For the first route the tumor is red and the entry point is A. The second route is restricted by the presence of blood vessels that should not be touched and has the tumor (blue) with entry at point B.

Figures 5 and **6** show that the deformation of the needle for both routes. We see that the deformation is small with no tendency to chaos. The strains are described
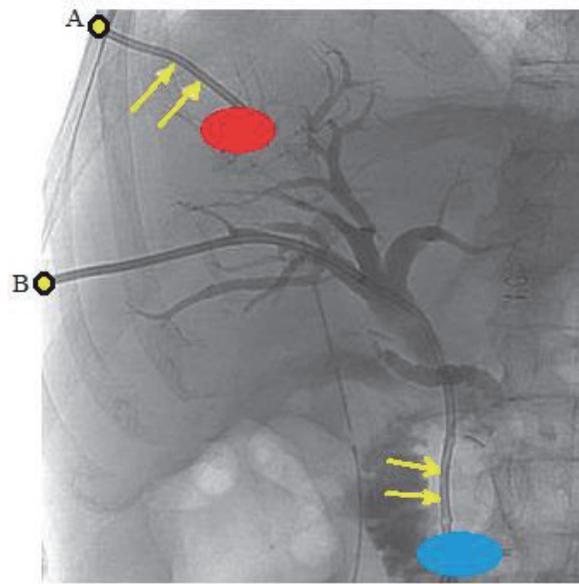

Figure 4.
Two needle trajectories: For first route the tumor is red and the entry point A, and for the second route tumor is blue and the entry point B.
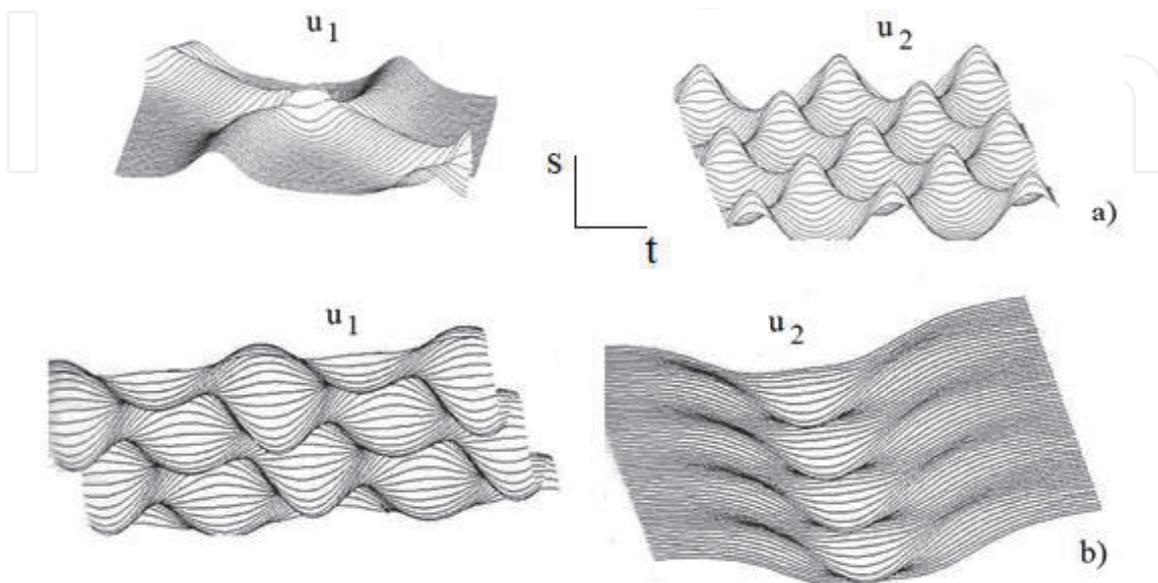

Figure 5.
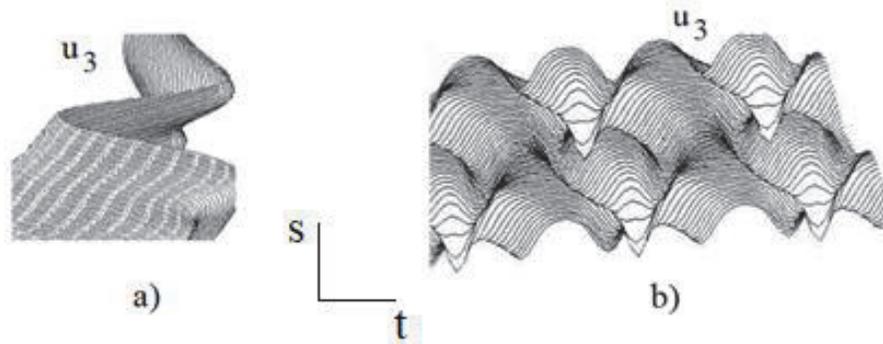*Functions u_1 and u_2 for a) first route and b) second route.*

Figure 6.
Function u_3 for a) first route and b) the second route.

by localized solitons which propagate for a long time without changes. The soliton is a localized wave with an infinite number of degrees of freedom. This wave conserves its properties even after interaction with another wave. In short, this wave acts somewhat like particles [43]. The system of Eqs. (7–11) has unique properties. These properties are locally preserved such as an infinite number of exact solutions expressed in terms of the Jacobi elliptic functions or the hyperbolic functions, and the simple formulae for nonlinear superposition of explicit solutions.

3. Determination of the free-collision trajectories

Let us present a model for determining the collision-free trajectories by using the Fibonacci sequence. The trajectories are determined from the restrictions of avoiding the collisions with blood vessels, ribs and surrounding tissues, and also the interference of needles with each other. We consider that more needles are planned to be inserted into the liver [45].

The trajectory of each needle $j = 1, \ldots, n$, is defined as a set of segments connecting the insertion point with the tumor. Two binary control parameters are introduced on each needle. The first parameter is the length of the kth segment of the jth needle's trajectory, $l_{kj} = f_k / r^{kj}$, where f_k is the kth Fibonacci number and r_{kj} a scaling number. The second control parameter is the angle ω between the current needle and the previous one, $\omega \in (0, \pi)$ [46, 47].

The sequence terms in the Fibonacci problem are 1, 1, 2, 3, 5, 8, 13, 21, 34, 55, 89, 144. It is clear that each term is a sum of two preceding sequence term. In fact, the sequence can be recursively defined in the form $f_n = f_{n-1} + f_{n-2}, f_0 = 0, f_1 = 1$. The limit of the ratio of two consecutive terms in the Fibonacci string tends to the gold ratio $\varphi = (1 + \sqrt{5})/2$ [48, 49].

The Fibonacci sequence was highlighted in nature for example in the arrangement of the flower petals, in seeds and in the spiral arrangement of pine cones and pineapple. The keys on a piano are divided into Fibonacci numbers, and numerous classical compositions implement the golden section. Such an example is found in the Alleluia Choir in Handel's Messiah and in many of Chopin's preludes [50].

Development of a target drug delivery technique usually consisted of three steps. In step 1, a 2D ultrasound image of the tumor is obtained. The size and position of the tumor are analyzed by the surgeon who decides the number of required needles. In step 2, the insertion points on the skin of the needles and the positions of the targets in the tumor are established. In step 3, once the needles are placed at the target points on the skin, they are guided according to a precise surgical planning
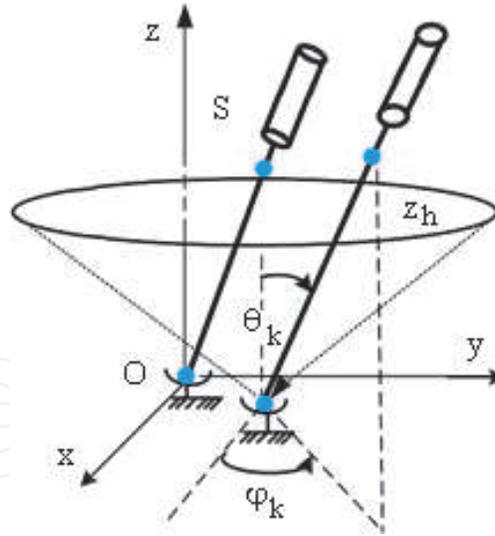
Figure 7.
The base coordinate frame.

based on the optimization of the collision-free trajectories to avoid the ribs, blood vessels and tissues in the abdominal area.

The base coordinate frame is established on the first needle with the vertical axis Oz and the origin in the insertion point (**Figure 7**). The workspace boundary for the needle is a 1D curve in each xy- plane means the z_h-plane for $z = h$, $h \in [0, h_{\max}]$ with a clinical value $h = 200$ mm. The S is the plan of the needle insertion trajectory, (θ_k, φ_k) are the rotation angles with respect to y and z axes $\theta_{\min} \leq \theta_k \leq \theta_{\max}$, $\phi_{\min} \leq \varphi_k \leq \varphi_{\max}$ [45].

The first control parameter is the length of the kth segment of the jth needle, $l_{kj} = f_k / r^{kj}$, $k = 1, \ldots, m_{lk}, j = 1, \ldots, n$ where f_k is the kth Fibonacci number

$$f_0 = f_1 = 1, f_{k+2} = f_{k+1} + f_k, k \geq 0. \tag{29}$$

and r_{kj} a scaling number. The second control parameter is the angle φ between the current needle and the previous one, $\varphi \in (0, \pi)$. The kinematic constraint of the jth needle, $j = 1, \ldots, n$, is given by

$$\phi = \begin{bmatrix} x_j - x_{0j} - \delta_{xj} - (h - z_{0j} - \delta_{zj}) \tan \theta_j \cos \varphi_j \\ y_j - y_{0j} - y_{yj} - (h - z_{0j} - \delta_{zj}) \tan \theta_j \cos \varphi_j \end{bmatrix} = 0, \tag{30}$$

where $\left[x_{0j} + \delta_{xj}, y_{0j} + \delta_{xj}, y_{0j} + \delta_{xj} \right]^T$ is the actual target of the tip of needle $(j - 1)$, $\left(\theta_j, \varphi_j \right)$ are the rotation angles with respect to y and z axes $\theta_{\min} \leq \theta_j \leq \theta_{\max}$, $\phi_{\min} \leq \varphi_j \leq \varphi_{\max}$ and $(\delta_{xj}, \delta_{yj}, \delta_{zj})$ denote the deformation of the liver.

The choice of the scaling number r_{kj} is done by a binary control

$$l_{kj} = \|x_k - x_{k-1}\| = \frac{u_{kj} f_k}{r^{kj}}. \tag{31}$$

The possible collision point between the needle and the tissue is analyzed by an identifier to check the minimum distance between needle and the surrounding tissue [45]. The minimum distance is expressed as

$$\min \left(\frac{1}{2} (r_1 - r_2)^T (r_1 - r_2) \right), \tag{32}$$

with $g_1(r_1) \leq 0$, $g_2(r_2) \leq 0$, r_1, r_2, the position vectors of two points belonging to the needle and the tissue, respectively, and g_1, g_2, the surfaces to the needle and the tissue, respectively. The interference distance or penetration is defined as

$$\min (-d), \quad g_1(r_1) \leq -\frac{d}{2}, \quad g_2(r_2) \leq -\frac{d}{2}, \tag{33}$$

where d is the penetration. The configuration of the collision-free trajectories of each needle is defined as a sequence of trajectories corresponding to a particular choice for the control (u, v). The set of all collision-free trajectories are computed based on the kinematic constraint (30) as

$$R = \left\{ \sum_{k=0}^{n} \frac{u_k f_k}{r^k} \exp \left(-i\omega \sum_{j=0}^{k} v_j \Big| (v_j) \in \{0, 1\} \right) \right\}. \tag{34}$$
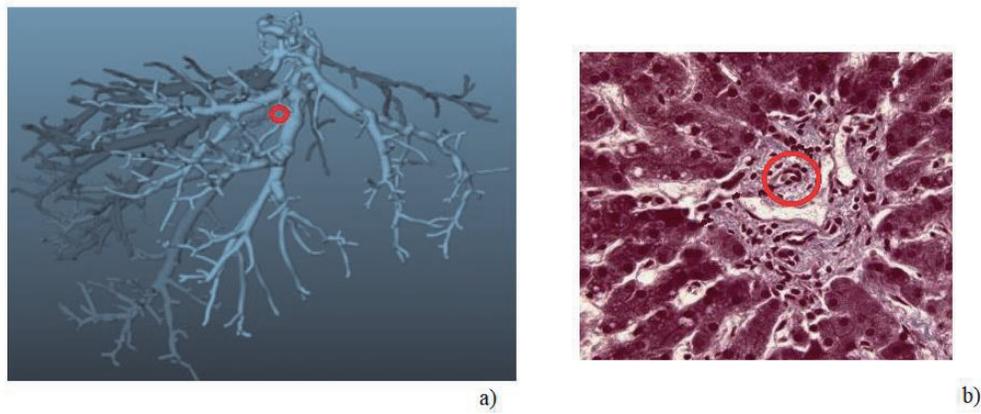

Figure 8.
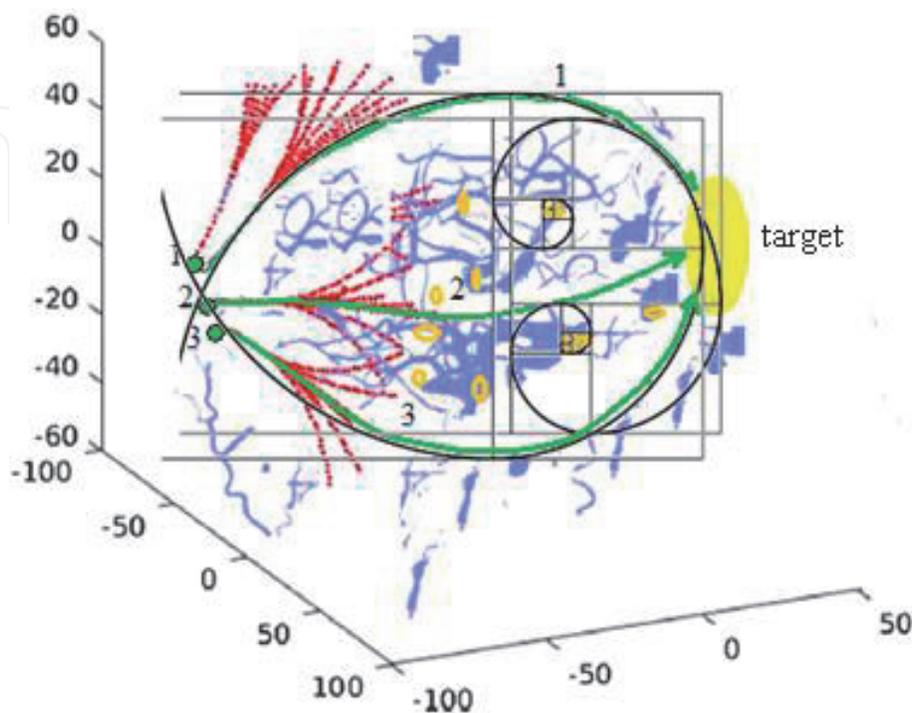*a) Location of the tumor; b) tumor image seen on the microscope.*

Figure 9.
Simulation of the collision-free trajectories for three-needles.

As application, the case of a tumor with a difficult location in the vicinity of the portal tree of the vascular territory in the liver, is considered (**Figure 8a**). The tumor image seen on the microscope is shown in **Figure 8b**. White and gray denote forbidden areas while the shade of purple are safe regions. The tumor is drawn in red. The Fibonacci algorithm is applied to three-needles with restrictions to avoid the collision with the tissues, blood vessels, ribs and previously inserted needles.

The task of our simulation is to determine the boundaries of each needle as a collision-free surface which represents the feasible insertion area based on given constraints. Then, the optimal trajectory of each needle can be chosen in this surface automatically.

Once all needles are placed at the predetermined epidermis and the ordering of entry is chosen to be 1, 2 and 3, following the first needle's insertion, the operation is repeated for the needles 2 and 3.

Simulation of the collision-free trajectories for three needles is presented in **Figure 9**. The insertion scheme is determined by the Fibonacci spirals. A set of free-collision trajectories (red) in the immediate vicinity of the epidermis, is suggested.
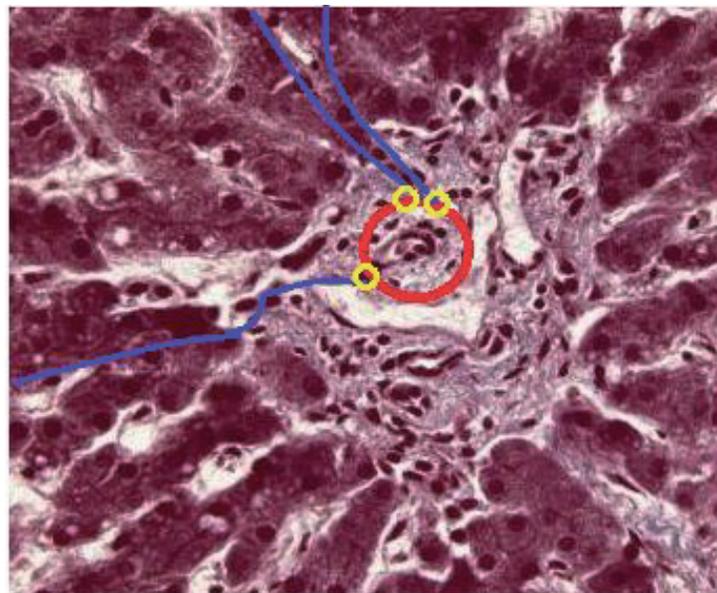

Figure 10.
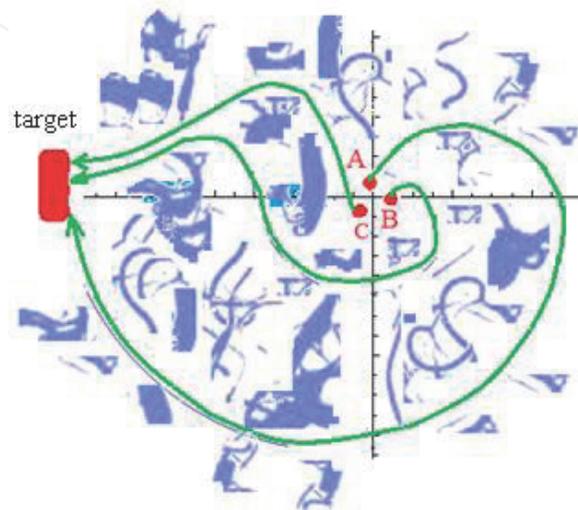*Optimal solution with 3 collision-free trajectories to the target.*

Figure 11.
Three optimal collision-free trajectories for the needle robot.

From these possible collision-free trajectories (red) the green paths corresponding to the Fibonacci spirals (black) are chosen. These trajectories avoid the blood vessels (purple) and the coasts (brown) in all directions until the tumor. Optimal solution with 3 collision-free trajectories to the target is displayed in **Figure 10**. The Fibonacci spirals with the centers in ribs (brown) are displayed for needles 1 and 3. For the needle 2, the Fibonacci.

Three locally optimal collision-free trajectories for the surgical needle corresponding to three different entry points into the skin A, B and C are displayed in **Figure 11**.

4. Conclusions

The study investigates the navigation of a flexible needle into the human liver. The role of the needle is to deliver into the tumor an active chemotherapeutic agent. The deformation of the needle during its insertion into the human liver is describe in this chapter in the context of intraoperative treatment of liver tumors based on the integrated imaging-molecular diagnosis. The needle is a bee barbed type modeled as a flexible thread within the framework of the Cosserat (micropolar) elasticity theory. The Cosserat elasticity describes the interaction between the needle and the human liver by incorporating the local rotation of points and the couple stress as well as the force stress representing the chiral properties of the human liver.

Acknowledgements

Conflict of interest

The authors of this paper certify that they have no affiliations with or involvement in any organization or entity with any financial or nonfinancial interest in the subject matter or materials discussed in this manuscript.

Author details

Veturia Chiroiu*, Ligia Munteanu, Cristian Rugină and Nicoleta Nedelcu
Institute of Solid Mechanics, Romanian Academy, Bucharest, Romania

*Address all correspondence to: veturiachiroiu@yahoo.com

IntechOpen

References

[1] Chiroiu, V., Nedelcu, N., Munteanu, L., Rugina, C., Ionescu, M., Dragne, C., *Modeling the flexible needle insertion into the human liver,* Proceedings of the Romanian Academy, series A: Mathematics, Physics, Technical Sciences, Information Science (2020).

[2] Sahlabadi, M., Hutapea, P., *Tissue defomation and insertion force of bee-stinger inspired surgical needles*, Journal of medical device, vol.12, 034501, 1–3 (2018).

[3] Dionigi, R., *Medical Intelligence Unit*: *Recent Advances in Liver Surgery*, Landes Bioscience Austin, Texas (2009).

[4] Dremin, V., Potapova, E., Zherebtsov, E., Kandurova, K., Shupletsov, V., Alekseyev, A., Mamoshin, A., Dunaev A., *Optical percutaneous needle biopsy of the liver: a pilot animal and clinical study*, Scientific Reports, volume 10, Article number: 14200 (2020).

[5] Abolhassani, N., Patel, R., Moallem, M., *Control of soft tissue deformation during robotic needle insertion*, Minimally Invasive Therapy, 15(3), 165–176 (2006).

[6] Abolhassani, N., Patel, R., Moallem, M., *Needle insertion into soft tissue: A survey*, Medical Engineerings & Physics, 29, 413–431 (2007).

[7] Torzilli, G., Minagawa, M., Takayama, T., *Accurate preoperative evaluation of liver mass lesions without fine-needle biopsy,* Hepatology, 30(4), 889–893 (1999).

[8] Baker, N.E., *Emerging mechanisms of cell competition*, Nature Reviews Genetics (2020).

[9] Petrowsky, H., Fritsch, R., Guckenberger, M., De Oliveira, M. L., Dutkowski, P., Clavien, P.A., *Modern therapeutic approaches for the treatment of malignant liver tumours*, Nature Reviews Gastroenterology & Hepatology (2020).

[10] Gino van den Bergen, *Collision detection in interactive 3D environments*, Elsevier (2004).

[11] Okamura, A.M., Simone, C., O'Leary, M.D., *Force modeling for needle insertion into soft tissue*, IEEE Trans Biomed Eng., 51,1707–16 (2004).

[12] DiMaio, S.P., Salcudean, S.E., *Needle insertion modeling and simulation*, IEEE Trans Robot Automat., 19, 864–75 (2003).

[13] DiMaio, S.P., Salcudean, S.E., *Simulated interactive needle insertion*, Proceedings of the 10th IEEE Symposium on Haptic Interfaces for Virtual Environment & Teleoperator Systems, 344–51 (2002).

[14] Maurin, B., Barbe, L., Bayle, B., Zanne, P., *In vivo study of forces during needle insertions*, Scientific Workshop on Medical Robotics, Navigation and Visualization (MRNV04), Germany, Remagen, 415–422 (2004).

[15] Lombardo, J-C, Cani, M-P, Neyret, F., *Real time collision detection for virtual surgery*, Computer Animation (CA'99), May 1999, Geneva, Switzerland, pp.82–90 (1999).

[16] Zachmann, G., *Minimal hierarchical collision detection,* Proc. ACM Symposium on Virtual Reality Software and Technology (VRST), Hong Kong, China, 121–128 (2002).

[17] Brişan, C., Boantă, C., Chiroiu, V., *Introduction in optimisation of industrial robots. Theory and applications,* Editura Academiei, Bucharest (2019).

[18] Kataoka, H., Washio, T., Audette, M., Mizuhara, K., *A model for relations*

between needle deflection, force, and thickness on needle insertion, Proceedings of the Medical Image Computing and Computer-Assisted Intervention Conference, 966–974 (2001).

[19] Pisla D., Vaida, C., Birlescu I., Nadim, A.H., Gherman, B.,Corina Radu, Plitea N., *Risk Management for the Reliability of Robotic Assisted Treatment of Non-resectable Liver Tumors*, Appl. Sci., 10(1), 52 (2020).

[20] Birlescu I., Manfred, H., Vaida C., Plitea N., Nayak A., Pisla, D., *Complete Geometric Analysis Using the Study SE(3) Parameters for a Novel, Minimally Invasive Robot Used in Liver Cancer Treatment*, Symmetry, 11(12), 1491 (2019).

[21] Vaida, C., Plitea, N., Pisla, D., Gherman, B., *Orientation module for surgical instruments - a systematical approach*, Meccanica, 48(1), 145–158 (2013).

[22] Munteanu, L., Rugină, C., Dragne, C., Chiroiu, V., *On the robotic control based on interactive activities of subjects,* Proceedings of the Romanian Academy, series A : Mathematics, Physics, Technical Sciences, Information Science, 21(1), (2020).

[23] Chiroiu, V., Munteanu, L., Ioan, R., Dragne, C., Majercsik, L., *Using the Sonification for Hardly Detectable Details in Medical Images,* Scientific Reports, 9, article number 17711 (2019).

[24] Korayem, M.H., Nikoobin, A., Azimirad, V.,*Trajectory optimization of flexible link manipulators in point-to point motion*, Robotica, 27, 825–840 (2009).

[25] Chiroiu, V., Munteanu, L., Ioan, R., Mosnegutu, V., Girip, I., *On the dL algorithm for controlling the hybrid systems*, Acta Electronica, Special Issue Proceedings of the XXIXth SISOM, 60

(1–2), 58–65, Mediamira Science Publishing (2019).

[26] Chiroiu, V., Munteanu, L., Dragne, C., Știrbu, C., *On the diferential dynamic logic model for hybrid systems*, Acta Technica Napocensis - series: Applied Mathematics, Mechanics, and Engineering, 61(4), 2018.

[27] Majercsik, L., *On the dL control applied to a Stewart platform with flexible joints,* Romanian Journal of Mechanics, 4(1), 27–38 (2019).

[28] Motta, PM,*The three-dimensional fine structure of the liver as revealed by scanning electron microscopy*, Int. Rev. Cytol.,Suppl 6, 347–399 (1977).

[29] Ma, M.H., Biempica, L.,*The normal human liver cell*, Am. J. Pathol., 62, 353–370 (1971).

[30] Jackson RL, Morrisett JD, Gotto AM., *Lipoprotein structure and metabolism,* Physiol. Rev. 56, 259–316 (1976).

[31] Saxena, R., Theise, N.D., Crawford, J.M., *Microanatomy of the human liver-exploring the hidden interfaces*, Hepatology, 30(6), 1339–46 (1999).

[32] Si-Tayeb, K., Lemaigre, F.P., Duncan, S.A., *Organogenesis and development of the liver*, Dev. Cell.,18(2), 175–89 (2010).

[33] Yi–Je Lim, Dhanannjay Deo, Tejinder P. Singh, Daniel B. Jones, Suvranu De, *In Situ* Measurement and Modeling of Biomechanical Response of Human Cadaveric Soft Tissues for Physics-Based Surgical Simulation, Surg Endosc., 23(6), 1298–1307 (2009).

[34] Narayan, K.S., Steele, W.J., Busch, H., *Evidence that the granular and fibrillar components of nucleoli contain 28 and 65 RNA, respectively*, Exp. Cell. Res., 43, 483–492 (1966).

[35] Habenschus, M.D., Nardini, V., Dias, L.G., Rocha, B.A., Barbosa Jr. F. , Moraes de Oliveira, A.R., *In vitro enantioselective study of the toxicokinetic effects of chiral fungicide tebuconazole in human liver microsomes*, Ecotoxicol. Environ. Saf., 181, 96–105 (2019).

[36] Takahashi, M., Takani, D., Haba, M., Hosokawa, M., *Investigation of the chiral recognition ability of human carboxylesterase 1 using indomethacin esters*, Chirality, 32(1), 73–80 (2020).

[37] Cosserat, E., Cosserat, F., *Theorie des corps deformable*, Herman et Fils, Paris, 1909.

[38] Eringen, A.C., *Microcontinuum Field Theory*, volume II. Fluent Media, Springer, New York (2001).

[39] Eringen, A.C., Kafadar, C.B., *Polar field theories.* In A. C. Eringen,editor, Continuum Physics, volume IV, pages 1–75. Academic Press, NewYork (1976).

[40] Iesan, D., *Existence theorems in the theory of micropolar elasticity*. International Journal of Engineering Science, 8, 777–791 (1970).

[41] Iesan, D., *Existence theorems in micropolar elastostatics*, International Journal of Engineering Science, 9, 59–78 (1971).

[42] Forest, S., Sievert, R., *Nonlinear microstrain theories*, International Journal of Solids and Structures, 43(24), 7224–7245 (2006).

[43] Munteanu, L., Donescu, St., *Introduction to Soliton Theory*: *Applications to Mechanics,* Book Series Fundamental Theories of Physics, vol.143, Kluwer Academic Publishers, Dordrecht, Boston (Springer Netherlands) (2004).

[44] Chiroiu, V., Munteanu, L., Gliozzi, A.S., *Application of the Cosserat theory for modeling the reinforcement carbon nanotube beams*, CMC: Computers, Materials & Continua, 19(1), 1–16 (2010).

[45] Dragne, C., Chiroiu, V., Munteanu, L., Brişan, C., Rugină, C., Ioan, R., Stănescu, N-D, Stan, A.F., *On the collision free-trajectories of a multiple-needle robot based on the Fibonacci sequence,* New Trends in Mechanism and Machine Science, Volume 89 of the Mechanisms and Machine Science series, Chapter 20 pp.1–12 Springer (2019).

[46] Lai, A.C., Loreti, P., Velluci, P.: A Model for Robotic Hand Based on Fibonacci Sequence. In: Proceedings of the 11th International Conference on Informatics in Control, Automation and Robotics (ICINCO-2014), pp.577–584 (2014).

[47] Aghili, F., Parsa, K.: *Design of a reconfigurable space robot with lockable telescopic joints*. In Conference IEEE/RSJ, International Conference on Intelligent Robots and Systems (2006).

[48] Burton, D. M.: *Elementary number theory* (5th ed.). New York: McGraw-Hill (2002).

[49] Fox, W.P.: Fibonacci Search in Optimization of Unimodal Functions. Department of Mathematic Francis Marion University, Florence, SC 29501 (2002).

[50] Silverman, J. H.: *A friendly introduction to number theory*. (3rd ed.) Upper Saddle River, NJ: Pearson Education (2006)